AD-A140 016 PLASMA THEORY AND SIMULATION(U) CALIFORNIA UNIV 1/1
BERKELEY ELECTRONICS RESEARCH LAB C K BIRDSALL
31 DEC 82 N00014-77-C-0578

UNCLASSIFIED F/G 20/9 NL

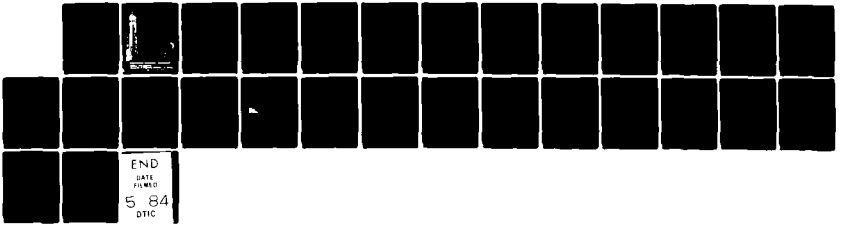

END
DATE FILMED
5 84
DTIC

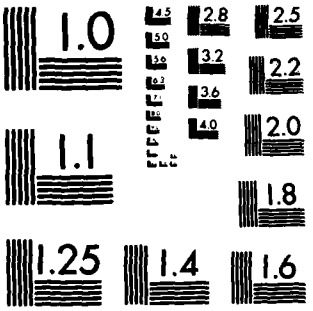

MICROCOPY RESOLUTION TEST CHART
NATIONAL BUREAU OF STANDARDS-1963-A

THIRD & FOURTH QUARTER PROGRESS REPORT
on
PLASMA THEORY AND SIMULATION

July 1 to December 31, 1982

This document contains papers about the use of

Our research group uses both theory and simulation as tools in order to increase the understanding of instabilities, heating, transport, and other phenomena in plasmas. We also work on the improvement of simulation, both theoretically and practically.

Our staff is –

Professor C.K. Birdsall*	191M	Cory Hall	(642-4015)
Principal Investigator			
Dr. Thomas L. Crystal	119ME	Cory Hall	(642-3477)
Post-Doctorate; Lecturer, UCB			
Dr. Bruce Cohen	L630	LLNL	(422-9823)
Dr. A. Bruce Langdon	L477	LLNL	(422-5444)
Dr. William Nevins	L630	LLNL	(422-7032)
Lecturers, UCB; Physicists LLNL			
Dr. Mary Hudson		SSL	(642-1327)
Guest, UCB; Senior Fellow, Space Science Lab.			
Dr. Siegbert Kuhn	119ME	Cory Hall	(642-3477)
Guest at UCB;			
Physicist, Univ. of Innsbruck, Austria			
Mr. Kwang-Youl Kim			
Mr. William Lawson			
Mr. Niels Otani			
Mr. Stéphane Rousset			
Mr. Vincent Thomas			
Mrs. Amy Wendt			
Research Assistants	119MD	Cory Hall	(642-1297)
	119ME	Cory Hall	(642-3528)

December 31, 1982

DOE Contract DE-AT03-76ET53064-DE-AM03-76SF00034
ONR Contract N00014-77-C-0578

ELECTRONICS RESEARCH LABORATORY

University of California
Berkeley, California 94720

** On leave at California Institute of Technology, Pasadena CA 91125 as Visiting Chevron Professor of Energy, March 1 to August 31, 1982 (host W. B. Bridges).*

TABLE OF CONTENTS

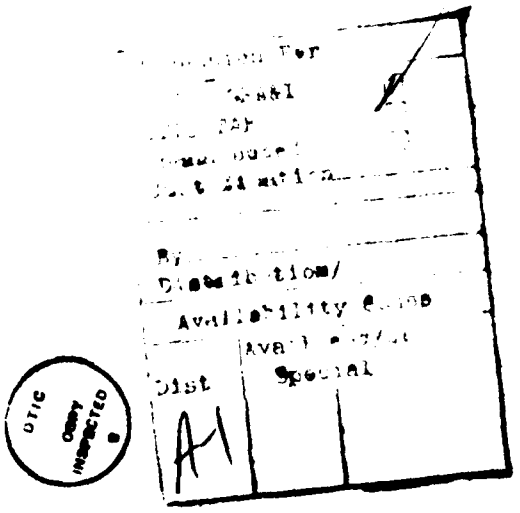

• Indicates ONR supported areas

SECTION I: PLASMA THEORY & SIMULATION

A. Electrostatic Ion-Ion Two Streaming Instability in a Thermal Barrier Cell

V. A. Thomas (Dr. W. M. Nevins, LLNL)

A report on this project is in preparation for publication.

B. Low Frequency Electromagnetic Ion-Streaming Instabilities

V. A. Thomas

I. Introduction

Many studies have been directed at instabilities arising from ion beams counter streaming along the field lines as in Refs. 1-2 and the references in Ref. 2. In particular, low frequency electromagnetic instabilities may arise in the following situations; (1) neutral beam injection parallel to the magnetic field, (2) runaway ions in a tokamak as in Ref. 3, (3) steady-state tokamaks sustained with neutral beam injection as in Ref. 4, (4) the counter streaming torus reactor concept as in Ref. 5, and (5) various space physics applications such as shocks. Ion-beam instabilites may also be important in some tandem mirror designs. Simulation studies of low frequency electrostatic streaming instabilities are quite numerous whereas the same cannot be said of low frequency electomagnetic streaming instabilities. Our goal is to examine some aspects of some of the situations indicated above.

II. Preliminary Results

In this section we present some initial results for the restricted case of propagation parallel to the ambient magnetic field. The simulation code has fully nonlinear ions and fluid electrons and uses the Darwin approximation together with quasineutrality to solve for the field quantites. The code was developed by N. Otani from an algorithm from D. Harned as in Ref. 6. The code is able to solve 2-½ dimensional problems with the ambient magnetic field in an arbitrary direction. For these test cases we use the code in a 1-d,3v periodic form.

Our test case consists of the problem considered in Ref. 7, the problem of cold counter-streaming ion beams with arbitrary relative density. The streaming direction is the same as the direction of the ambient magnetic field and we use the center-of-momentum frame of reference. The plasma is also charge neutral. Then making the Darwin approximation of negligible transverse displacement current and neglecting the electron inertial effects we obtain, as in Ref. 7

$$\left[\frac{k^2c^2}{\omega_{pi}^2}\right] - \frac{\omega}{\Omega_{ci}} + 1 - F1(\omega,k) - F2(\omega,k) = 0.$$

where

$$F1(\omega,k) = \frac{(1-\eta)\Omega_{ci}}{\omega + \eta \mathbf{k}\cdot\mathbf{U} + \Omega_{ci}}$$

and

$$F2(\omega,k) = \frac{\eta\Omega_{ci}}{\omega - (1-\eta)\mathbf{k}\cdot\mathbf{U} + \Omega_{ci}}$$

Here c is the speed of light, η is the ratio of the less dense ion beam particle density to the electron density, ω_{pi} is the ion plasma frequency calculated using the total ion density , and U is the relative drift between the two ion beams.

In Fig. 1 and Fig. 2 we compare linear growth rates and real frequencies for two cases from Ref. 7. The agreement between simulation and theory is quite good. The parameters for our simulations were $\Omega_{ci}\Delta t = 0.01$, $ng = 64$, and $np = 2000$. The beams were initially cold and only the first Fourier mode was retained.

III. Future Directions

In the future we plan to examine the nonlinear consequences of some of these instabilities and the various processes important for stability. Also it may be necessary to perform simulations that include propagation at an angle to the magnetic field so as to the include the instability with the lowest threshold as explained in Ref. 1. This unstable mode is an Alfvén mode in contrast to the mode presented in this paper which is a magnetosonic mode. The saturation levels for these two modes need to be examined carefully.

References

1. E. A. Foote and R. M. Kulsrud, *Phys. Fluids* 24 , 1532 (1981).
2. F. W. Perkins, *Phys. Fluids* 19 , 1012 (1976).
3. Z. G. An, Y. C. Lee, and C. S. Liu, *Univ. Maryland, Report number* 82-093 (Oct. 1981).
4. D. R. Mikkelsen and C. E. Singer, *Princeton Report* PPPL-1929 (Sept. 1982).
5. T. H. Stix, *Nuclear Fusion* 15, 545 (1972).
6. D. S. Harned, *J. Comput. Phys.*47 , 3 (1982).
7. K. I. Golden, L. M. Linson, and S. A. Mani, *Phys. Fluids*, 16 ,2319 (1973).

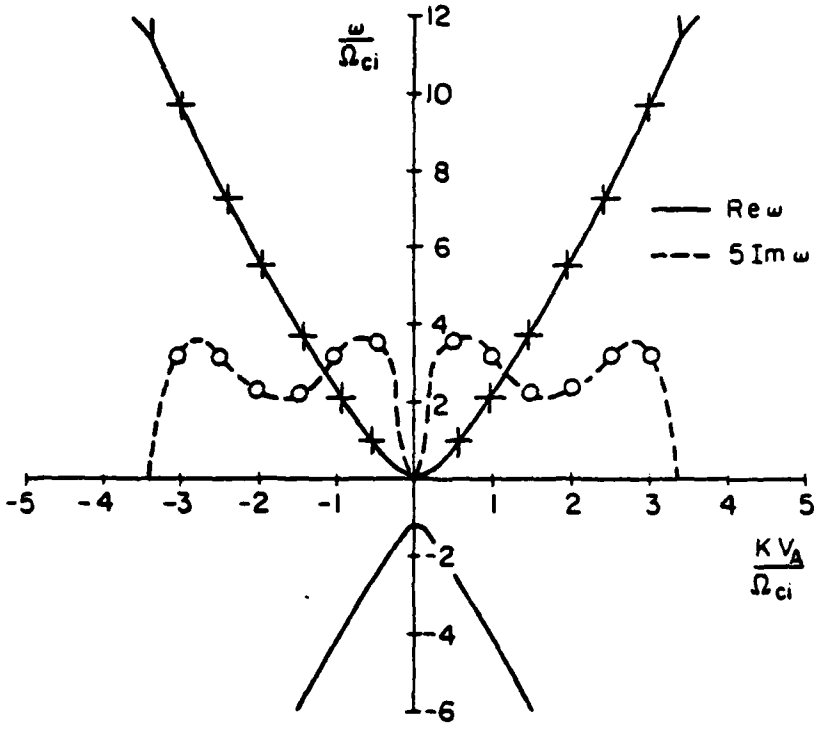

FIG. 1. Growth rates and real frequencies for the case of two equally dense counter streaming beams, $\eta = 0.5$. For this case $U/V_A = 7$. The crosses and the dots represent the simulation values for the real frequency and the imaginary part of ω.

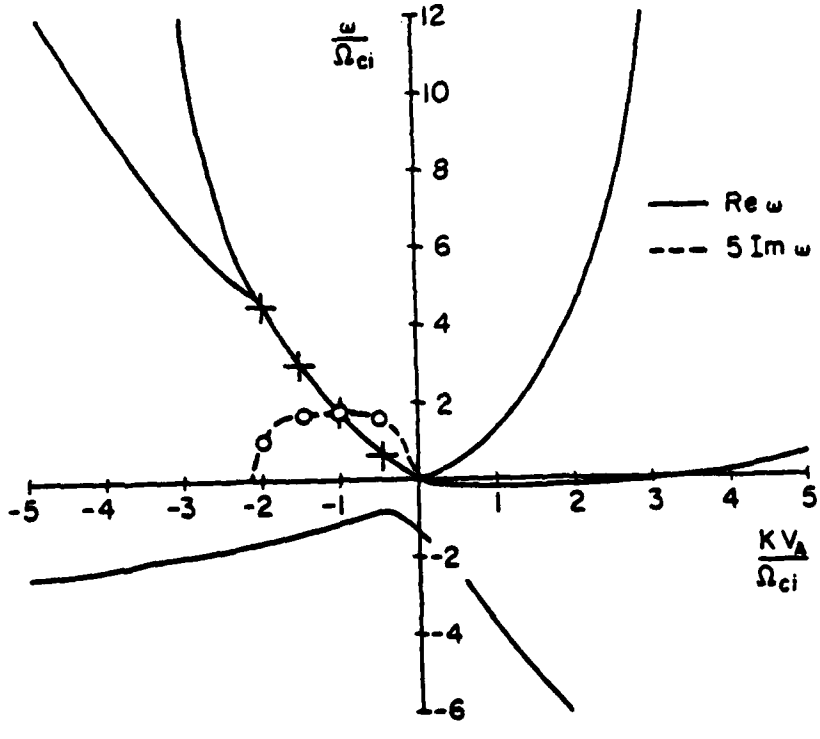

FIG. 2. Growth rates and real frequencies for the case $\eta = 0.1$ and $U/V_A = 3$.

SECTION I: PLASMA THEORY & SIMULATION

C. Alfvén Ion Cyclotron Instability Particle Simulations

Niels F. Otani (Dr. G. R. Smith, LLNL)

Details of the progress made in our study of the Alfvén ion-cyclotron instability for the period covered by this publication will be presented as part of a later report, currently in preparation. Four constants are calculated for the motion of ions in a single, purely transverse wave propagating along a uniform magnetic field. A simple, physically intuitive derivation of the AIC dispersion relation is presented using an infinite fluid representation of the standard Vlasov phase-space fluid. These results are used in the analysis of computer simulations of the instability. Simulations to this point have employed "four-spokes" ion distribution functions similar to those described in a previous QPR,[1] generalized by the inclusion of several parallel velocity beams to model finite $T_{i\parallel}$. Two separate simulation codes are being used. TRACY, a one-dimensional magneto-inductive code has already been described.[1] Additionally, a new, two-dimensional quasineutral Darwin algorithm has been written, and will be detailed in the next QPR. Currently, this code is being used to check the results being produced by TRACY, and is therefore being run as a one-dimensional code. Linear growth rates observed in both codes agree well with those predicted theoretically for continuous bimaxwellian distributions for $\beta_{i\perp} \gtrsim 1$, in the vicinity of the peak of the growth spectrum. Discrepancies in the growth rates for larger values of k and smaller $\beta_{i\perp}$ are discussed with the help of numerical solutions to the dispersion relation for 1) multibeam distribution functions and 2) continuous bimaxwellian distribution functions. Observations of particle trapping and other modifications to the ion distribution near wave saturation are explained in terms of the approximate constants of the particle motion.

[1] *Third Quarter Progress Report on Plasma Theory and Simulation.* July 1, 1981 - Sept. 30, 1981.

SECTION I: PLASMA THEORY & SIMULATION

D. Theory of Asymmetric Double Layers

K. Y. Kim

An ERL Report Memo with this title exists, with abstract as follows:

We present analytic solutions for asymmetric double layers which satisfy the time stationary Vlasov-Poisson system and which require a double valued Sagdeev potential as a function of physical potential: it is pointed out that any distribution function having an analytic density representation as a polynomial power series of potential can never satisfy the asymmetric double layer boundary conditions. K-dV like equation is found showing a relationship between the speed of asymmetric double layer and the degree of asymmetry.

E. Kinetic Equations and the Effects of Electron-Plasmon Coupling on Electromagnetic Wave-Plasma Interaction

K. Y. Kim (Prof. C.K. Birdsall and Dr. T.L. Crystal)

An ERL Report with this title is in preparation, with abstract as follows:

We have obtained the coupled equations for the electron and plasmon distribution functions, taking into account the multiphoton effect and the nonlinear enhancement of plasmons in the presence of an electromagnetic wave. By using a time dependent unitary transformation, the nonlinear damping rate by electron-plasmon coupling is calculated non-perturbatively with respect to the electromagnetic field intensity.

F. Plasma Surface Interactions

Prof. C. K. Birdsall
(work done at IPP, Nagoya, Japan and Cal Tech, Pasadena)

(1) **Introduction**: Plasmas and surfaces (walls) interact in a great variety of ways. The plasma near the wall forms a sheath which may be rather far from electrically neutral relative to the body of the plasma. The sheath region may extend a few Debye lengths into the plasma, or a few hundred Debye lengths. The wall may absorb and emit particles in a variety of ways and may also be coupled to external sources and circuits, both active and passive. The particle penetration in the wall may range from zero to a few atomic layers to many layers. Knowledge of the physics and chemistry of the volume and surface interactions is of interest scientifically and for applications such as fusion first walls, space ship charging, and industrial processing.

The current state of knowledge of plasma-surface interactions may be termed fair theoretically and experimentally with a very extensive literature, but yet not wholly satisfactory. What happens to the standard models with $T_e >> T_i$ when the ions are made warm, with T_i comparable to T_e, and/or KT is in the keV ranges as in fusion devices? What is the detailed volume and surface physics and chemistry in plasma ("dry") etching? Are the time-independent and low-frequency answers sufficiently close to the time average of the time-dependent behavior, especially in light of known large amplitude nonlinear and possibly turbulent sheath behavior? There are many questions yet to be answered.

Computer simulation using particles (and/or fluids also, where appropriate) is well suited to explore the time-dependent plasma behavior in plasma-wall interactions, where the plasma is not neutral, non-Maxwellian, possibly in a large amplitude state, with both fluid-like and particle-like waves existing together. The wall behavior may also be explored using particles for example; the plasma-surface model may be considered as two or more adjacent plasmas, each with characteristic scale lengths and times, having electrons and ions and neutrals (atoms, molecules).

(2) **Acknowledgements**: This research is relatively new to us and was begun in cooperation with the Institute of Plasma Physics, Nagoya University, Nagoya, Japan. C. K. Birdsall was at IPP from September 1, 1981 until February 28, 1982 (on leave), with a short visit in September 1982, working with Dr. T. Kamimura and programmer Y. Ohara on plasma sheath simulations during the second half of this period, as reported herein. Prof. Birdsall is grateful to Dr. Kamimura for being a gracious host and for providing the excellent services of Mr. Ohara, who made setting up the sheath simulation work a real pleasure, and for partial support from the Japan Ministry of Education, through IPP. We plan on continuing joint research in this area of plasma-wall interactions, as a long-term cooperative project, with additional personnel exchanges and including the possibility of a computer link, Nagoya to California. Part of the diagnostics of the results was done at California Institute of Technology, with thanks to my hosts Profs. W. B. Bridges, R. W. Gould, and to the Chevron Research Co. for my support as Visiting Professor; Brian Leahy did the programming.

(3) **Related Areas -- Bibliography**: Plasma-surface interactions with large and fluctuating potentials, tend to be related to other examples of large potentials in plasmas, such as: formation and fluctuations in double layers and in virtual cathodes and virtual anodes; free expansion of a warm plasma; launching and propagation and decay of very large amplitude waves (BGK, solitons, etc.); thermal barriers (really potential barriers or wells in tandem mirror fusion devices). The author took advantage of the excellent library and library personnel at IPP, Nagoya to locate a representative group of references in these related areas. An informal report[1] lists these references which is intended to encourage others to become informed of the many past efforts. We make no claim to being exhaustive, or locating the definitive works, or identifying the inventors. The preparation was mainly for a small informal seminar (held November 20,21 1981 at Biwa-Ko in Japan) where we chose to list experiments and simulations where the time-dependent plasma-wall behavior (say, near ω_{pe} and ω_{pi}) played an important role in the overall plasma behavior. The work to follow here has a similar built-in slant:

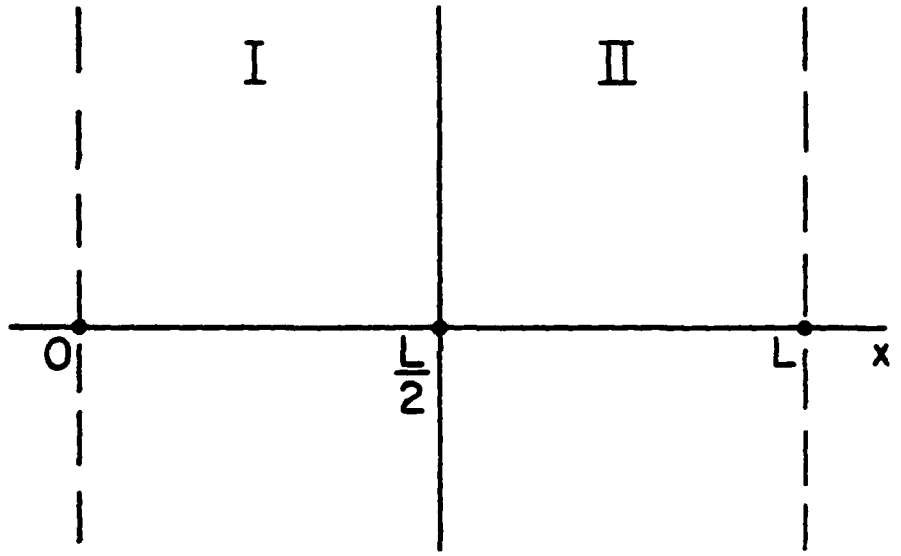

Figure 1. Model for floating wall sheath simulations. The RAM model has particles only in region I, $0 < x < L/2$, reflected at $x = 0$ and absorbed at $x = L/2$. The charge density is mirrored about $x = L/2$ (but not inverted) with the potential solved for over $x = 0$ to $x = L$ (no particles in region II, $L/2 < x < L$). $E = 0$ at $x = 0, L/2, L$. The density of particles collected at $x = 0, L/2$ is doubled. The RAR model has particles over the whole region, $x = 0$ to $x = L$, with particles reflected at $x = 0$, absorbed at $x = L/2$ and reflected at $x = L$. Both RAM and RAR models produce potentials that are symmetric about $x = L/2$. The model is periodic, period L.

caveat emptor. The references given by *Name (date)* may be found in the reference[1].

(4) **Initial Objective -- Sheath Formation, and Steady State**: A first object is to look carefully at the formation of the sheath and subsequent steady state (if there is one) in a plasma near a planar absorbing wall or probe. The steady state commonly found in time-independent analyses uses warm electrons which follow a Boltzmann relation (implying $m_e \rightarrow 0$) and cold ions. Solutions are found only for ions drifting into the sheath regions with a velocity equal to or greater than the acoustic velocity v_s; ions are presumably accelerated to v_s in a pre-sheath region many Debye lengths long called the pre-sheath; there is negligible electron density next to the wall where Child's Law applies (for space-charge-limited ion currents) describing ion acceleration into the wall. An objective is to compare solutions of this nature with the time-average of our time-dependent results.

(5) **Initial Model**: The model chosen is a uniform plasma put in contact with an absorbing wall at $t = 0$. Cipolla and Silevitch (1981) solve this time-dependent model with a fluid-ion Boltzmann-electron analysis. Denavit (1979) treats a uniform warm plasma slab which is allowed to expand freely after $t = 0$, using ion and electron particle simulation. These two one-dimensional models are related in that the absorbing wall which is unconnected (floating) collects charge and creates an electric field in the plasma similar to that of the charge that has escaped from the expanding plasma. Both articles provide thorough physical and mathematical descriptions and extensive references to prior work which, of course, extends back 50 years to Langmuir.

The model which we simulate is an initially spatially uniform warm plasma bounded by an absorbing wall (connected by a resistor R to ground, but with $R \rightarrow \infty$, floating) at one side and a charge reflecting plane at the other side, as shown in Figure 1. The model period is L, twice the separation between reflecting plane and absorbing wall; either the plane or the wall may be considered the center of the whole period. The charge density is mirrored across the absorbing wall, but not inverted. $E = 0$ at $x = 0$ (no surface charge) and at $x = L/2$ (by symmetry, but open to question). Both ions and electrons are represented by particles, starting with non-drifting Maxwellian distributions in v at $t = 0$. The floating wall absorbs particles crossing the wall boundary and remains charged with them. After a long time the plasma eventually decays to the wall; there is no reinsertion of particles. With T_e much larger then T_i, the wall very quickly becomes charged negatively (in about 3 τ_{pe}), reflecting most electrons, and accelerating the ions that are nearby, subsequently collecting electrons and ions in very nearly equal numbers. This behavior is expected from elementary physics. However, the wall potential ϕ_w is observed to have large amplitude fluctuations at the plasma frequency with the time average of ϕ close to but not exactly equal to the floating potential expected from elementary time-independent analysis. The details of the progress made so far are now given.

(6) **Typical Parameters -- Prototype for Warm Electrons, Cool Ions, $T_e \gg T_i > 0$** : The model length L needed to observe the physics is typically on the order of or larger than 100 Debye lengths, $L \geq 100\lambda_{De}$. The cell size Δx needed for numerical stability is something like a third of a Debye length or smaller, $\lambda_{De}/\Delta x \geq 1/3$. These choices indicate use of $L \geq 300\Delta x$ or more. The number of particles per cell needed to keep the particle (shot) noise small is about 5 to 10; the number needed per Debye length to keep the essence of the plasma physics is also about 5 to 10; hence, the total number of particles needed is on the order of a few thousand. These minimal parameter requirements are met easily and economically; observation of subtle effects requires many more particles.

The oscillation time scales are the electron plasma period and the much longer ion sound wave and ion plasma periods. Hence, the time step is chosen to be on the order 1/15 of a plasma cycle, $\omega\Delta t = 0.4$. One long time scale met is the ion sound wave transit time over the system length, $T = L/v_s$; the other is the ion thermal transit time $T = L/v_{ti}$. For mass ratio $m_i/m_e = 400$, electron thermal speed $v_{te} = 1.0$, $v_{sound} \equiv v_{te}\sqrt{m_e/m_i} = 0.05$, so that the transit

[1] C.K. Birdsall "Plasma-Sheath-Wall Time-Dependent Behavior: An Informal Survey," ERL Memo. UCB/ERL M82/51 June 22, 1982.

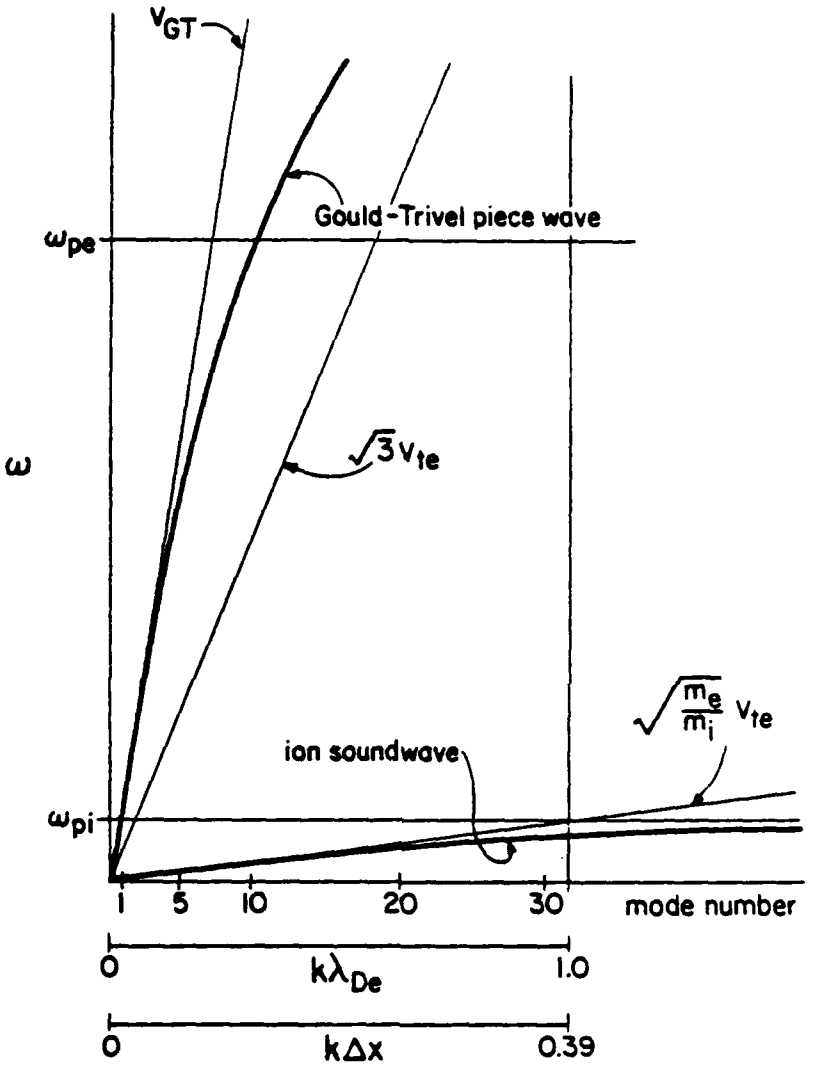

Figure 2. Dispersion diagram for L/R = 100 (L = $100\lambda_{De}$, R = $10\lambda_{De}$) for mass ratio of 100, $T_e \gg T_i$.

time is $T = 100\lambda_D/(v_{te}\sqrt{m_e/m_i} = 100/\omega_{pi} \approx 16\tau_{pi}$; this is about $300\tau_{pe}$ or $\omega_{pe}T = 2000$ or about 5000 time steps. This is a long time to run. One way around is to make the mass ratio smaller (at $m_i/m_e = 100$ the run length drops by 2). Another way is to use an implicit particle moving scheme with much longer time steps, to be used only after achieving assurance that short wavelength and high frequency effects may be ignored, an assumption not yet gained. Hence, using a 10μsec/particle/step computer, with 10^4 particles and 5000 steps, runs will be 500 seconds long, about 8 minutes. Our initial runs are for 500 steps, lasting less than a minute on the FACOM 230 Fujitsu machine at IPP; restart capability is being worked out, to do 500 steps at a time. For ease of reading results, we set $v_{te} = 1.$, $\omega_{pe} = 1.0$ making $\lambda_{De} = 1.0$. Also using $(q/m)_e = -1.0$ makes $e\phi/KT_e = e\phi/(m_e v_{te}^2) = \phi$; that is, ϕ is already in units of $e\phi/KT_e$. Typically $L = 200$ so that the active region used is $L/2 = 100\lambda_{De}$. With 512 cells, $\lambda_{De}/\Delta x \approx 2.5$.

(6) **Dispersion for the Simulations**: The $\omega - k$ dispersion is shown in Figure 2 for $m_i/m_e = 100$, $T_i << T_e$. The lower branch is the ion acoustic wave. The upper branch is the Gould-Trivelpiece wave which is forced on the system by replacing

$$\omega_p^2 \quad \text{by} \quad \omega_p^2(\ ) = \omega_p^2 \frac{k^2}{k^2 + k_\perp^2}, \quad k_\perp \equiv \frac{2.405}{R}$$

Here R is inferred to be the radius of *disk* charges rather than *sheet* charges (for which $R \to \infty$). The reason for forcing this dispersion is somewhat obscure, having to do with observing large amplitude oscillations in ϕ_{wall} (to be described shortly) and wondering if these oscillations drive large amplitude waves, e.g., solitons, which require normal (nondecay type) dispersion.

Separate simulations with one species with excitation localized in space and lasting about τ_p indeed show nonlinear waves, with zero crossings propagating away from the region of excitation at very nearly

$$v = (\omega_p^2/k_\perp^2 + v_{te}^2)^{1/2} \equiv v_{GT}$$

which is the $(\omega, k \to 0)$ speed for Gould-Trivelpiece waves.

Our simulations are done with $L/R = 10$ ($L = 100\lambda_{De}$, $R = 10\lambda_{De}$) and also with $R \to \infty$; both "radii" produce grossly the same results. Of course, for $R \to \infty$, the upper branch is the usual Langmuir wave, with anomalous (decay type) dispersion.

(7) **Typical Results, for $m_i/m_e = 100$**: Typical results are shown in Figure 3 for $m_i/m_e = 100$, and $T_i/T_e = 10^{-4}$. These are snapshots taken at times 50,100,...,400, roughly every $8\tau_{pe}$ or $0.8\tau_{pi}$. (a) is ϕ vs x; the slanted line drawn on the output moves away from the absorbing wall at speed $v_s = v_{te}\sqrt{m_e/m_i} = 0.1$, at about the first zero-crossing of ϕ (a little meaningless as ϕ is not fixed at either $x = 0 or L/2$). (b) is the electron velocity distribution $f(v_e)$ over the whole plasma showing loss of the faster electrons and a squaring up of $f(v_e)$. (c) is electron phase space showing both a cooling and shrinking near the wall, with boundary region also moving to the left at about v_s. (d) is $f(v_i)$ with tick marks at v_s, showing beginnings of beams late in time. (e) is ion phase space, same v_s tick marks, showing expansion of the ion acceleration region at speed v_s.

Clearly it is desirable to have these pictures developed over much longer time. Perhaps the boundaries moving at v_s reach $x = 0$ (the center of the whole period) and then the ions drift to the wall at some speed on the order of v_s or v_{ti}. Runs with $m_i/m_e = 1$, $v_s = 1.0$ to time 200 and with $m_i/m_e = 4$, $v_s = 0.5$, to time 400 (both are two ion sound transit times) show something like this but with mean ion speed still increasing in space from $x = 0$ to $x = L/2$. However, as the electrons cool considerably (and hence v_s decreases) during the run (no reinsertion or heating is used), the ion sound may not have yet reached $x = 0$. Very long runs are needed.

(8) **Wall potential oscillations**: The potential of the floating wall, ϕ_{wall}, is shown in Figure 4 as a function of time, (over $400/2\pi \approx 64\tau_{pe}$). The dominant short period oscillations (period $\approx 20 \approx 3\tau_{pe}$) are those of mode 2 or 3 at $k\lambda_{De} < 0.1$, where no damping is expected.

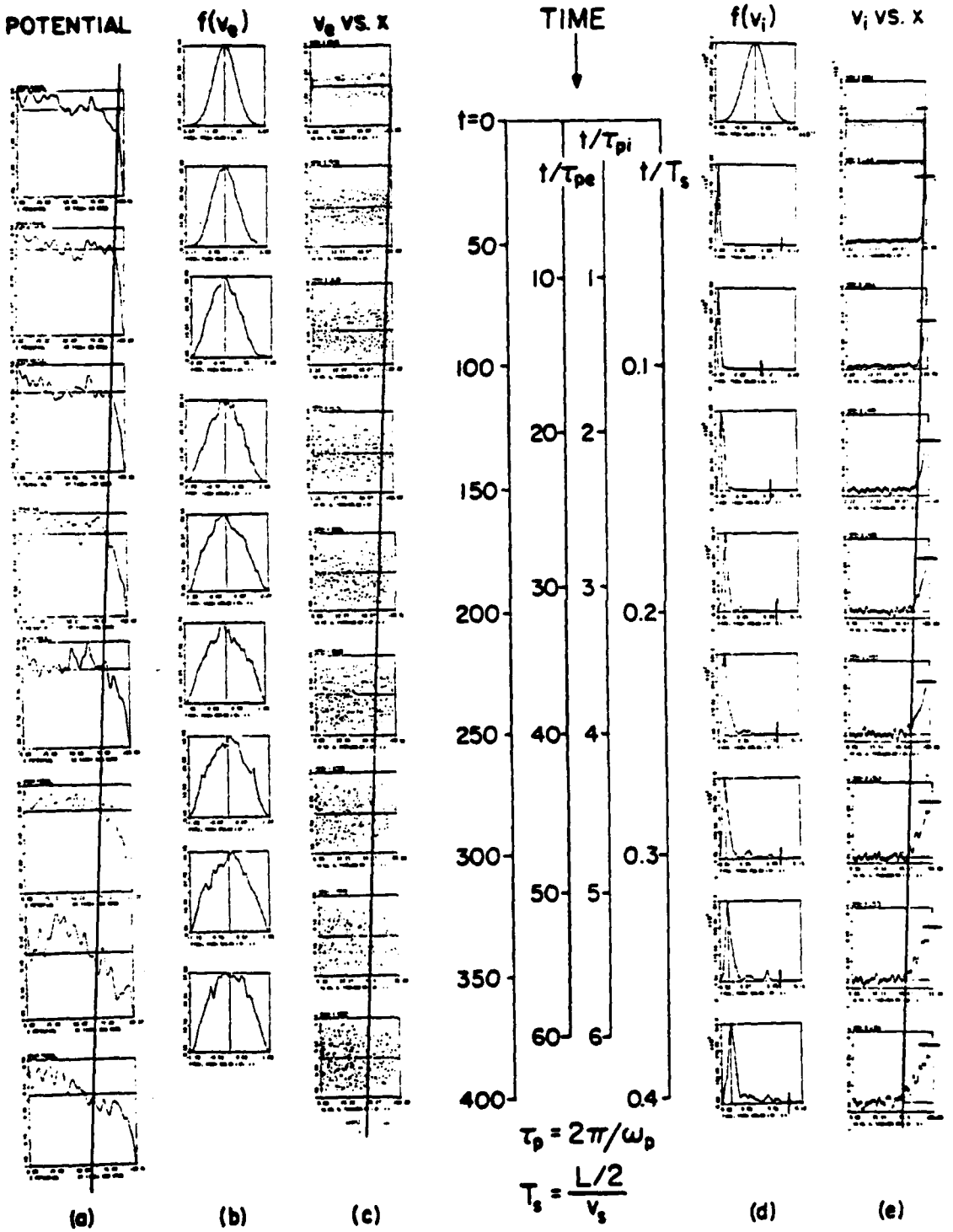

Figure 3. Early time history of the formation of the sheath at a floating wall. The distribution functions f(v) are averaged over all of the particles. The slanted lines correspond to ion sound velocity, showing a sound wave propagating away from the absorbing wall at roughly sound speed, in the potential and in f(v).

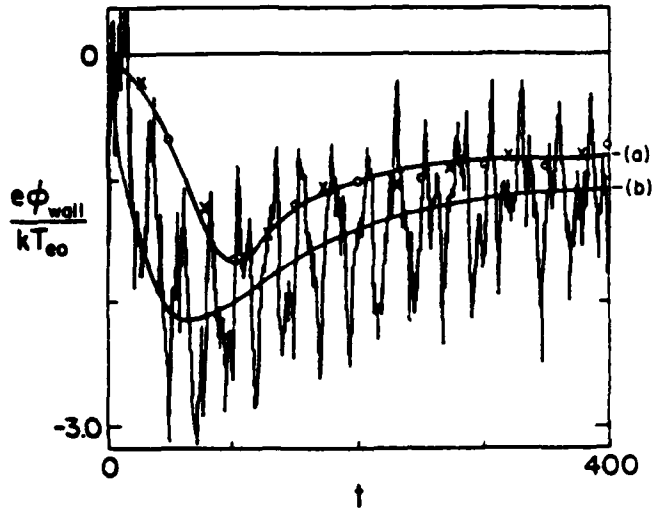

Figure 4. Potential at the absorbing wall versus time. The fast oscillations are plasma oscillations. Curve (a) is the kinetic energy of an ion absorbed at the wall ($m_i v_i^2/2$). Curve (b) is a running average of ϕ_{wall}. The minimum value near t = 60 is about

$$-\tfrac{1}{2}\ln(m_i/m_e) + 0.25 = -2.05 \quad (for\ m_i/m_e = 100)$$

as expected from static theory, for $T_e \gg T_i$. After t = 100, electrons with $v > v_t$ have free streamed at least 0 to L, with many collected, so that ϕ rises.

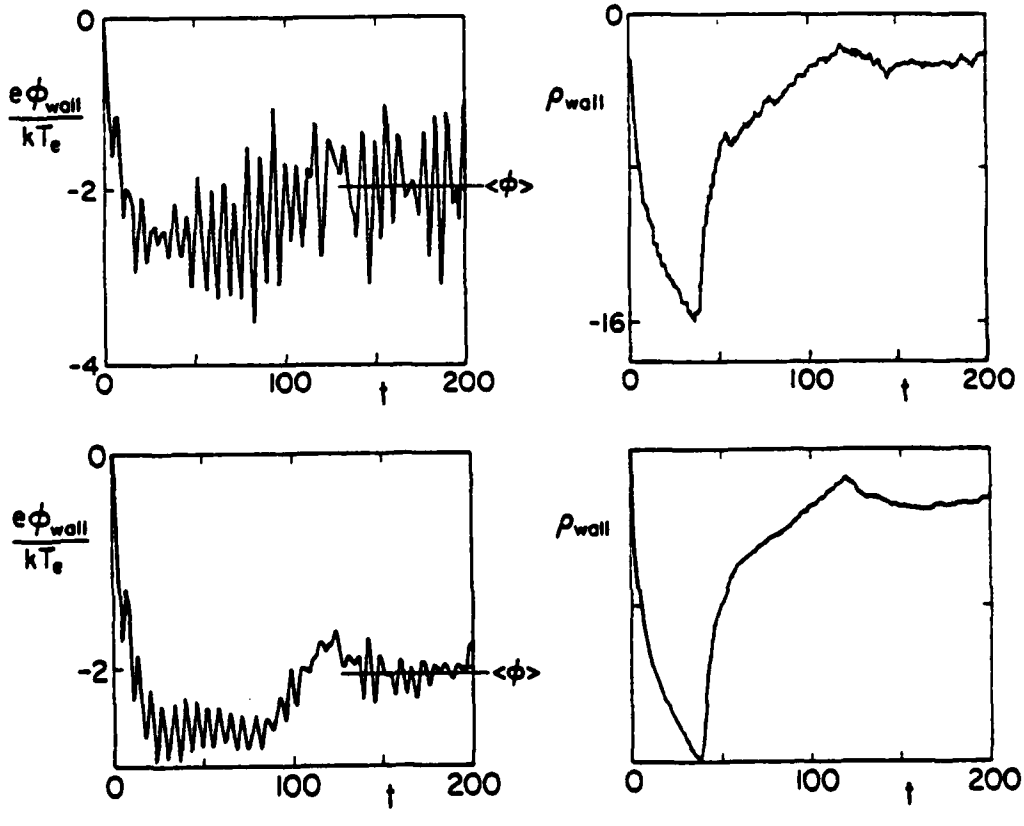

Figure 5. Model results using Langmuir dispersion (R→∞, 1d sheets) first for $N_e = N_i = 4096$, then 32,768 particles, mass ratio 400, $T_e \gg T_i$. The mean ϕ_{min} near $t^i = 30$ to 80 is close to the expected value from statics, - 2.75. Note the diminution of plasma oscillation amplitude as N increases, but with al most no change in ρ_{wall}.

The points on curve (a) are for the kinetic energy of the ions absorbed at the wall; the circles are at $t = 50, 100, \cdots 400$, and the x's are averages over $t = 0$ to 50, 50 to 100, $\cdots$ 350 to 400. Curve (b) is an estimate for the running time average of ϕ. The difference between (a) and (b) starts at about $\Delta(e\phi/KT_e) \approx 1$ and drops to about 0.5 later; this is expected to be zero in time-independent analysis (the ions are accelerated from rest in this time period). Due to $\partial\phi/\partial t \neq 0$, we cannot expect $(\frac{1}{2} m v_i^2 + q_i \phi_i)$ to be constant.

In runs with radius $R \to \infty$ (Langmuir dispersion), the dominant oscillations in ϕ are at ω_p (as determined from measurements using different mass ratios, down to $m_i/m_e = 1$) and not at $(\omega_p^2 + k^2 v_t^2)^{\frac{1}{2}}$, hence at $k\lambda_D \leq 0.1$ where no damping is expected. Typical results are shown in Figure 5, ϕ_{wall} and ρ_{wall} (essentially the surface charge density), as dependent on time, for $m_i/m_e = 400$, $T_e >> T_i$. The results for $N_i = N_e = 4096$ show larger oscillations in ϕ_{wall} than seen for $N_i = N_e = 32{,}768$ particles. However, $e<\phi>/KT_e \approx 2$ near $t = 200$ in both runs; overlaying the two curves of ρ_{wall} shows only smoothing as N is increased, with no gross change. The transient in ρ_{wall} shows electron collection until $t \approx 30$, when the first ion is collected, then recovery to an oscillating state. We suspect that there may be low frequencies (e.g., $\omega \leq \omega_p$) present in ϕ_{wall} and ρ_{wall} requiring longer runs to resolve. We suspect further that there may be intermittent electron-then-ion oscillation bursts as postulated by us when working with oscillating virtual cathodes in electron diodes (Birdsall and Bridges, 1961). These were seen by Cutler experimentally (1964) and examined in detail by Culter and Burger (1966) in simulations and experiments. See also articles by Burger (1964, 1965, 1967) and others as given in the survey mentioned earlier. Resolution of these effects usnig simulation (in part repetition of Burger's pioneering work, but with improved techniques of simulation, and more detailed diagnostics) requires many more particles and much longer runs, and introduction of a source and or re-insertion.

The overall behavior of a drop in ϕ to a minimum, followed by a slow rise rather than remaining at a minimum, is probably due to the early loss of the faster electrons (as noted by J. M. Dawson in a seminar). Hence, with a replenishing source supplying a full Maxwellian, the slow rise would not be expected. Thus, comparison with steady state expectations (such as Emmert *et al* [2]) are to be made at $\phi_{minimum}$; rough checks with [2] are good.

(9) **Energy Histories -- ion heating**: The active particle energy histories are shown in Figure 6 to accompany the earlier Figures 2, 3, 4. The active particles are in the region $0 < x < L/2$ (no particles $L/2 < x < L$) and the energies do not include the absorbed particles. The kinetic and thermal energy of the electrons halves, as the electrons give energy to the ions and the fields and are collected; at $t = 400$ about 16 percent of the electrons (and ions) have been absorbed. The drift energy of the electrons is relatively small, oscillating in time like ϕ_{wall}. The ion energies all increase in time to about one tenth that lost by the electrons. (The scales are correct as $KE_e(t=0) = \frac{1}{2} m n v_{te}^2 = 50$. The field energy is not shown, as it was obtained incompletely. Hence, there is no total energy check as yet.) The ion thermal energy shows an initial rise, apparently exponential, from $T_i/T_e = 10^{-4}$ to about 10^{-2}. If the growth in T_i is taken as $\exp(2\gamma t)$, then γ is measured to be $0.77\ \omega_p$. At $t = 0$, $\lambda_{Di}/\Delta x$ is 0.0256, growing exponentially to 0.256 at $T_i/T_e = 10^{-2}$, and a little larger later in time. This initial heating was observed further shown in Figure 7, for initial values of T_i/T_e up to about 0.25, for which $\lambda_{Di}/\Delta x = 1.$ Perhaps this growth is nonphysical, related to the well-known heating due to aliasing obs one-species Maxwellian for $\lambda_D/\Delta x \leq 0.3$.

(10) **Particle** les are lost from the plasma and absorbed by the wall at rates shown in Figure 8 of Figures 2, 3, 4, 6. N is the number of electrons or ions remaining in the plasma measured at times 0, 50, 100, $\cdots$ 400. (The rapid fluctuations are *not* shown.) The average difference $<N_i - N_e>$ is about 15 particles over most of the run, out of 2 x 4096 initially, or about 0.2 percent. 648 electrons and 633 ions are absorbed, about 16 percent of each. The average ion flux is thus $\Delta N/\Delta T = 633/400 = 1.58$. If the ion flux is

[2] G. A. Emmert, R. M. Wieland, A. T. Meuse, J. W. Davidson, "Electric sheath and presheath in a collisionless, finite ion temperature plasma", *Phys. Fluids* **23**, pp.803 - 812, April 1980

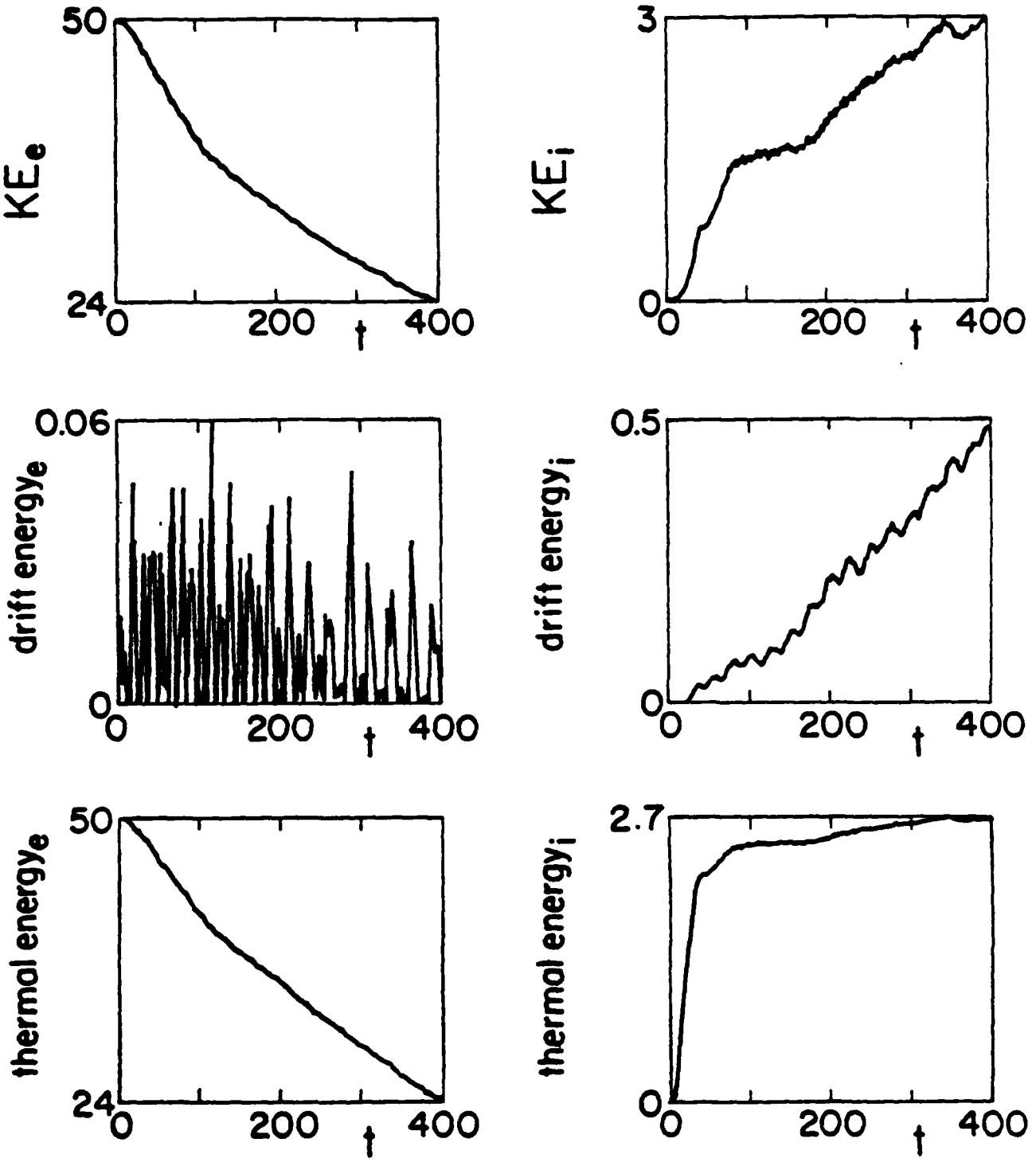

Figure 6. Various energies as a function of time. The loss of electrons (especially the faster ones) causes a drop in KE_e by a factor of 2. The ion kinetic and thermal energies show an early exponential rise (the latter is on a log scale, covering almost 3 decades) which may be numerical in origin (self-heating) due to very small initial λ_{Di}/x; as a result T_i/T_e rises by about 100 to where $\lambda_{Di}/x = 0.25$.

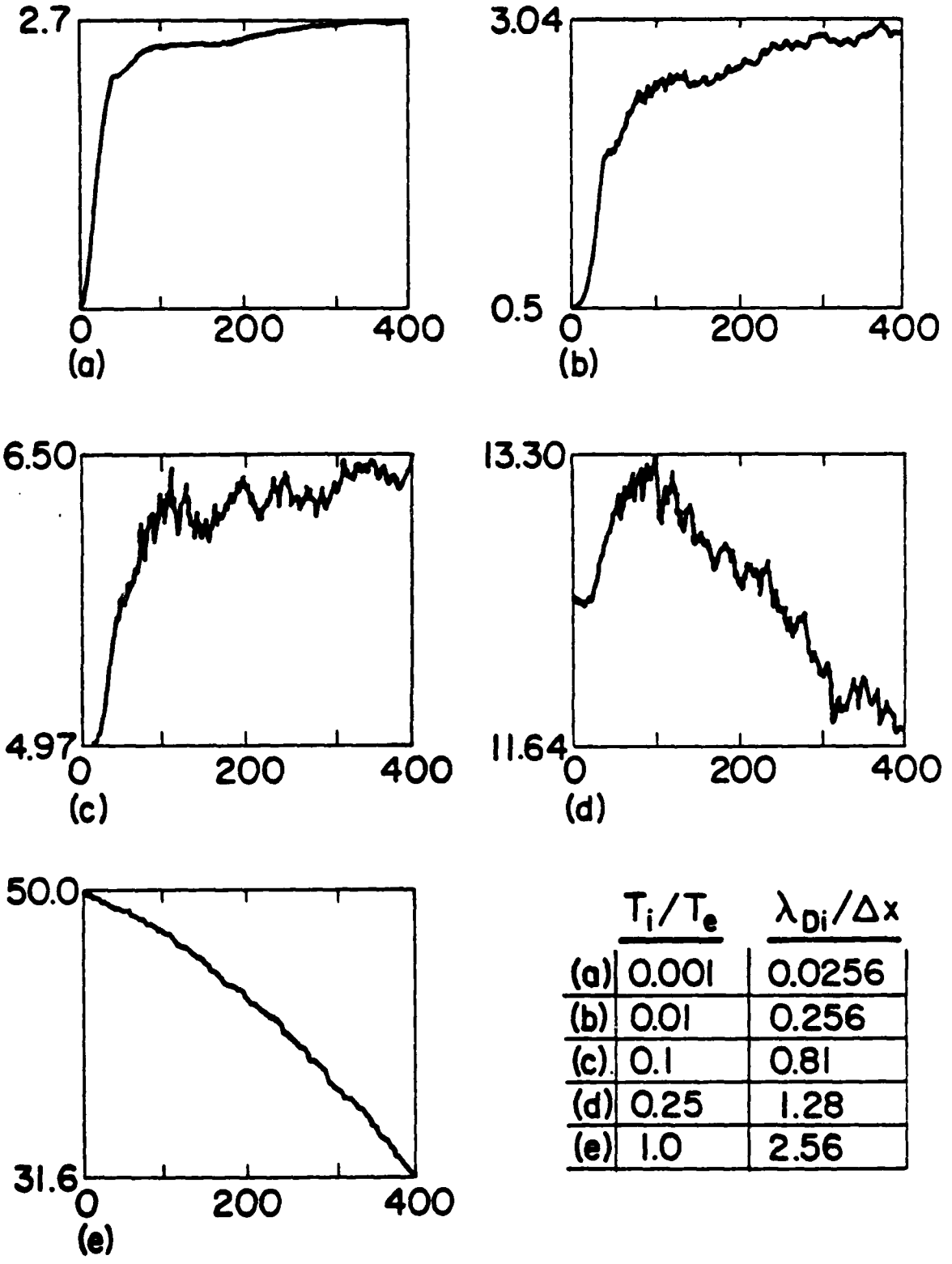

	T_i/T_e	$\lambda_{Di}/\Delta x$
(a)	0.001	0.0256
(b)	0.01	0.256
(c)	0.1	0.81
(d)	0.25	1.28
(e)	1.0	2.56

Figure 7. More details on the initial rise of ion thermal energy, as the initial T_i is increased, versus time. The ion energy scale is logarithmic. All for $m_i/m_e = 100$, $\lambda_{De}/\Delta x = 2.56$. The initial growth (probably numerical) turns to decay at large T_i, which is probably mostly loss of ions (not cooling).

taken as $(N/L)v_s = (4096/100)(0.1) = 4.096$, the result is too large, mostly due to using $n_{wall} = N/L$ which is much too large; the flow velocity at the wall is 1 to 2 times v_s.

(11) **Comparisons with simple time-independent analysis**: It is useful to make comparisons of these results with those obtained from time-independent analysis. We have already seen one such, between $(\frac{1}{2} m_i v_i^2)$ and $(q_i \phi)$ at the wall in Figure 4. Let $T_i << T_e$, essentially treating the ions as cold. Assume that the ions are accelerated from rest up to energy $q\phi_{wall}$ so that

$$(\tfrac{1}{2} m_i v_i^2)_{wall} = (-q_i \phi)_{wall}$$

not wholly inconsistent with Figure 3(a) and (e). Let the electrons be warm, following a simple Boltzmann factor density law. Assume that the electron and ion wall fluxes are the same, $\Gamma_e = \Gamma_i$, as

$$\Gamma_e = (\frac{n_o}{2})(v_{te}\sqrt{\frac{2}{\pi}})\exp(e\phi/KT_e) = n_o v_i = \Gamma_i$$

This relation does not account for density at the wall decreasing as electrons are repelled or as ions are accelerated. Replacing ϕ with $(-\frac{1}{2} m_i v_i^2/q_i)$ and KT_e with $m_e v_{te}^2$ produces the solution for $(v_i/v_{te})_{wall}$ vs m_i/m_e shown in Figure 9 labelled simple theory. The simulation results are shown as circles. The sound velocity $(v_s = v_{te}\sqrt{m_e/m_i})$ is also shown, substantially smaller than the simulations. The simulation results imply variation as $(m_i/m_e)^p$ where $p \approx 0.4$, not square root. The analysis comes from discussions with Dr. Allan Boozer at IPP, Nagoya.

Using the same simple theory, ϕ_{wall} is obtained and shown in Figure 10, compared with $<\phi>$ from simulations as indicated in Figure 5 (late in time, after some of the faster electrons have left). The time-independent result is about ½ unit smaller than that measured; this result is similar to that shown earlier in Figure 4 for $m_i/m_e = 100$. $<\phi>$ from simulations here is measured *after* the initial transient, near the end of the various runs (after 500 or 1000 steps). Another theory from [2] (their Eq. (35) or their Figure 4, for $T_i/T_e \to 0$) is

$$\frac{e\phi_{min}}{KT} \approx -\tfrac{1}{2}\ln\frac{m_i}{m_e} + 0.25$$

also shown in Figure 10. Using $<\phi>$ as ϕ_{min}, before too much loss of the faster electrons, would lead to better agreement with this latter theory. We have also done (Cal Tech) the double sheath boundary (floating boundaries at $x = 0, L$), not necessarily symmetric about L/2, and checked our early time ϕ_{min} vs m_i/m_e with [2] and found good agreement.

(12) **Ion wall speeds as T_i/T_e is increased**: The results with warm ions are only partially explored. One pressing question is the distribution of energies of the collected ions for $T_i \approx T_e$, as for fusion first walls. This is answered in Figure 11. For $T_i/T_e \leqslant 0.1$, (after the initial transient) all the ions are collected at 1 to $2v_s$, independent of T_i/T_e. For larger T_i/T_e, writing $v_s = v_{te}\sqrt{m_e/m_i}\ \sqrt{1 + T_i/T_e}$, the mean value of $(v_i/v_{te})_{wall}$ also is just larger than v_s. However, as soon as T_i/T_e exceeds about 1, the spread of velocities of collected ions increases. The quality of these runs decreases as T_i/T_e increases because of the more rapid decrease of particles remaining in the plasma. A source or reinsertion of particles is needed.

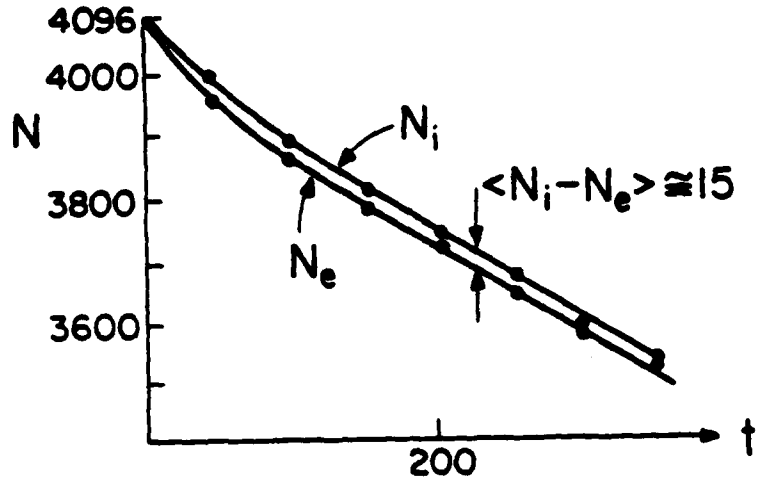

Figure 8. Total number of ions and electrons remaining in the system as a function of time, for 4096 of each at t = 0. Goes with Figures 2,3,4,6. Data taken at points shown; later data taken continuously is much the same (i.e., no clear-cut oscillations). (The data needed for such is flux, like dN/dt, not done yet.)

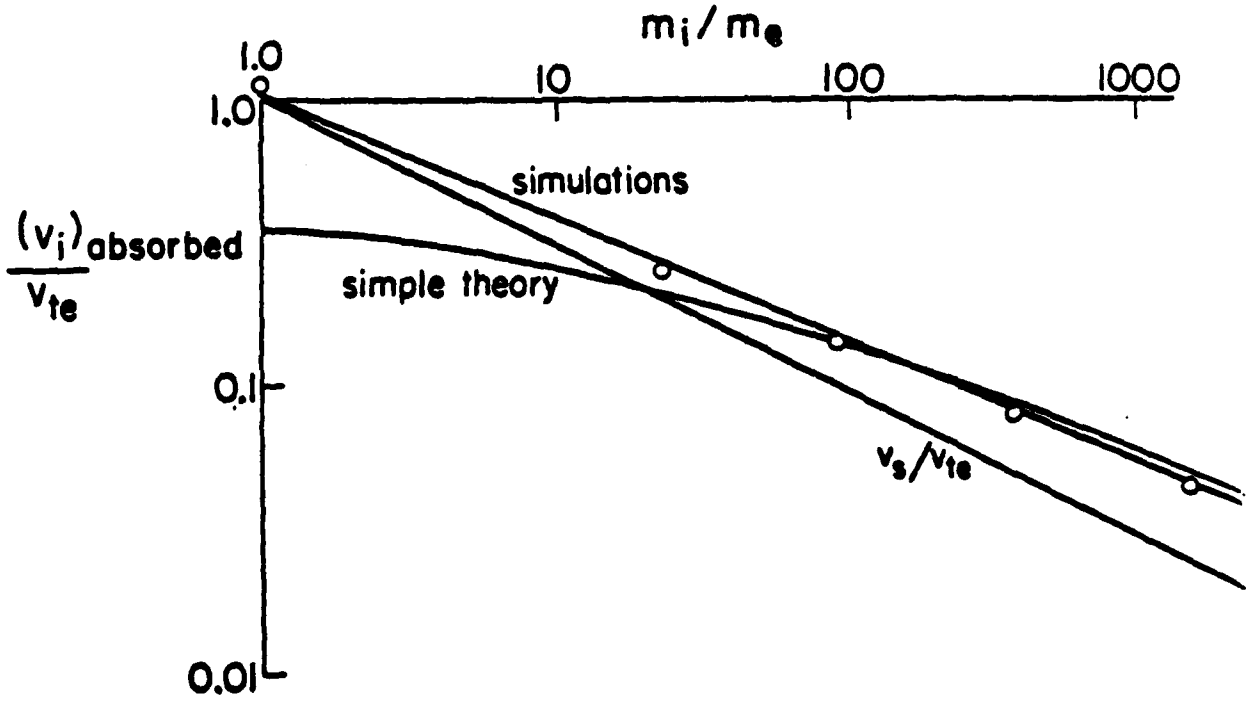

Figure 9. Speed of the ions at absorption versus mass ratio, with simulations shown as open circles.

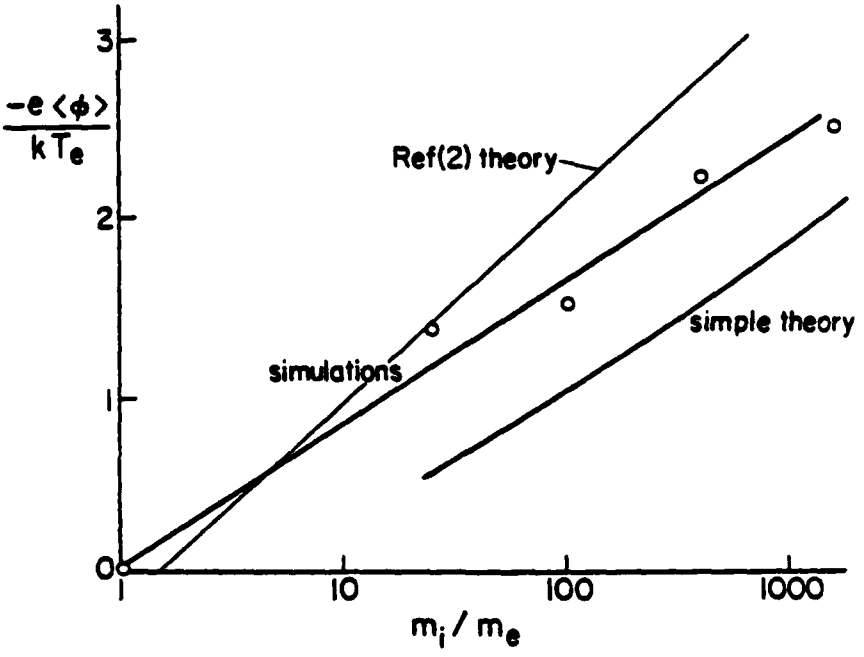

Figure 10. Wall potential taken at late times (after the faster e's are absorbed) as a function of mass ratio; the theory from Ref.(2) for $T_e \gg T_i$ is also shown.

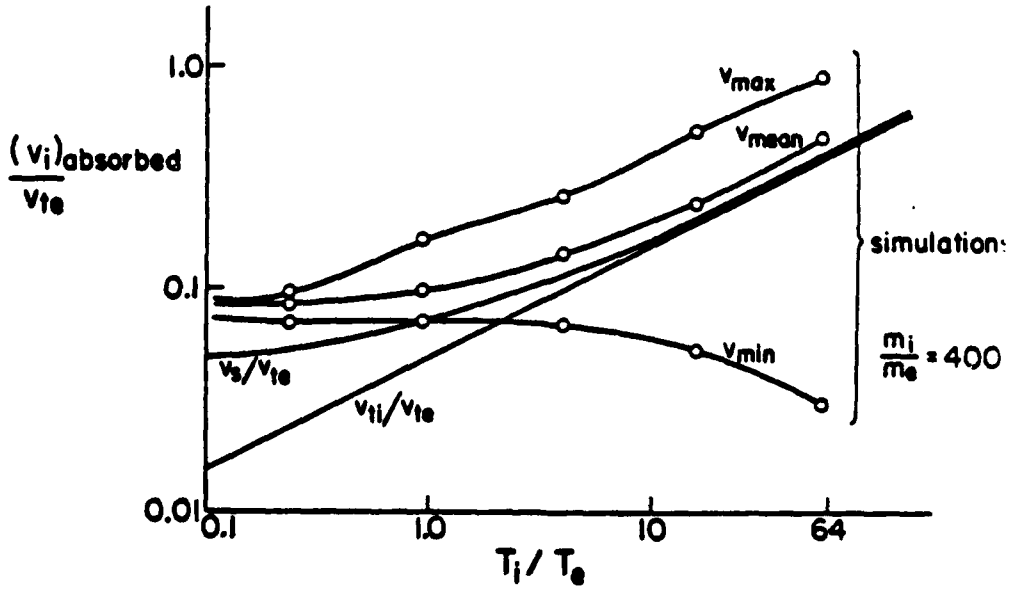

Figure 11 Ion velocity at absorption as a function of T_i/T_e for $m_i/m_e = 400$. The data become less reliable for increasing T_i due to more rapid loss of ions.

SECTION II: CODE DEVELOPMENT

Plasma Diode: 1-D Vlasov Simulation (GASBAG Code)

Wm. S. Lawson

Purpose

GASBAG is designed to solve electrostatic problems in one dimension with non-periodic boundary conditions. It solves the Vlasov equation on a grid $v_x - x$. It is being used to provide an independent check of results obtained by particle methods which are suspected of being numerical or noise effects.

Method

A non-periodic Vlasov simulation poses a major problem for grid solution, because there can be jump discontinuities in the distribution function, which no finite difference equation can adequately handle. To solve this problem, a (hopefully) continuous distribution function is introduced, and a string of test particles is used to keep track of where the discontinuity lies. This is a generalization of the Waterbag model used by Berk and Roberts[1]. This string of particles can be thought of as a line dividing a real distribution function from a fictitious distribution function.

These particles are moved using the standard leap-frog method, which is second order in time. A scheme for moving the distribution function which is compatible with this method of moving the test particles is the splitting scheme used by Cheng and Knorr[2]. This splitting scheme has the advantage that it can be used with any one dimensional method of interpolation (or finite difference approximations to the derivative).

Current Status

The code has been thoroughly debugged for a single species, and several new diagnostics have been added. Work has started on documentation, and a paper for publication. A poster presentation of the method was also given at the Tenth Conference on the Simulation of Plasmas.

The code is being used first in a perturbation study of the one dimensional diode (i.e. single species). The cathode emission distribution is perturbed, and the resulting current perturbations are observed. This is a first crude look at how noise affects the diode. The theory for this is difficult, since the problem (even the linearized problem) is non-linear.

Future Work

The GASBAG code is applicable to many interesting problems. Some possibilities are the study of the filling in of hole or trapped distributions, and the study of double layers.

References

1. H. L. Berk and K. V. Roberts, *Phys. Fluids* **10**(1967), 1595.
   K. V. Roberts and H. L. Berk *Phys. Rev. Letters* **101**(1967), 297.
2. C. Z. Cheng and Georg Knorr, *J. Comp. Phys.* **22**(1976), 330-351.

SECTION II: CODE DEVELOPMENT

B. Poisson Solver with Boltzmann Electrons

V. A. Thomas, A. B. Langdon (Prof. C. K. Birdsall)

A nontrivial problem in 1-d simulations is to obtain $\phi(x)$ from

$$\frac{d^2\phi(x)}{dx^2} = -e\,[\,n_i(x) - n_o\exp(e\phi(x)/T_e)] \qquad e>0 \tag{1}$$

where $n_i(x)$ is known (from particle or fluid equations) and constants n_o, T_e are given. The difficulty is with the exponential form of the Boltzmann electron density.

Langdon suggests an iterative scheme in which we expand around an approximated solution, as follows: Let $\delta\phi = \phi - \phi'$ where ϕ' is known from the last timestep or last iterate. Replace ϕ with $\phi' + \delta\phi$ in Eq.(1) to obtain (expanding the exponent to $O(\delta\phi)^2$)

$$\frac{d^2\delta\phi}{dx^2} - \left(\frac{n_o e^2}{T_e}\right)\exp(e\phi'/T_e)\,\delta\phi = -\left[\frac{d^2\phi'}{dx^2} + e\left(n_i - n_o\exp\left(\frac{e\phi'}{T_e}\right)\right)\right] + O(\delta\phi)^2 \tag{2}$$

Note that the left-hand side displays the local shielding with its λ_D^{-2} multiplier. The right-hand side is treated as a known source (ignoring terms $O(\delta\phi)^2$) so that $\delta\phi$ may be obtained directly from Eq.(2). Then having $\delta\phi$, use $\phi_{new}' = \phi_{old}' + \delta\phi$; repeat Eq.(2) and iterate this process through to convergence. Successive iterations yield decreasing $\delta\phi$'s, the corrections becoming ignorable as Eq.(1) is more closely satisfied: $\phi' \to \phi$. Care is needed particularly (i) at boundaries, (ii) concerning overall neutrality, and (iii) possible multiple solutions, as Eq.(1) is nonlinear. It is worth noting that the expansion scheme used in obataining Eq.(2) could be generalized to any $n_e(\phi)$ i.e., is not restricted to only exponential (Boltzmann) electrons.

Thomas uses a different scheme, taken from Mason [1]; this second "direct" scheme is also iterative but does not involve an expansion around an approximate solution. Start with

$$\nabla\cdot E = -e\left[n_o\exp\left(\frac{e\phi}{T_e}\right) - n_i\right] \qquad e>0 \tag{3}$$

In 1-d, take d/dx of Eq.(3) to obtain

$$\frac{d^2E}{dx^2} = -e\left[n_o\frac{e}{T_e}\frac{d\phi}{dx}\exp\left(\frac{e\phi}{T_e}\right) - \frac{dn_i}{dx}\right] \tag{4}$$

Replacing $d\phi/dx$ with $-E$, and $n_o\exp\left(\frac{e\phi}{T_e}\right)$ with $n_e = (e\,n_i - dE/dx)/e$, we obtain an equation in E without exponentials, which may be written as

$$E = \left[\frac{d^2E}{dx^2} - e\frac{dn_i}{dx}\right] \Big/ \left[\frac{e}{T_e}\left(en_i - \frac{dE}{dx}\right)\right] \tag{5}$$

This equation is put in finite difference form at timestep or iterate number n on grids numbered $1 \leqslant j \leqslant NG$, as

$$E_j^n = G(\,E_1^n, E_2^n \ldots E_{NG}^n, \text{other knowns}\,) \tag{6}$$

where G does *not* contain E_j^n. This means that dE/dx in Eq.(5) comes from points $j\pm1$, and

[1] R. Mason, "Computer Simulation of Ion-Acoustic Shocks. The Diaphragm Problem", *Phys. Fluids*, **14**, pp.1943-1958, Sept. 1971.

the E_j in d^2E/dx^2 is shifted to the left-hand side of Eq.(6). Using previous iterate values on the right-hand side, Eq.(6) with this shift is then solved for all E_j; assume either $E_j^n = 0$ for all j or use E_j^{n-1} to start. Mason uses $E = 0$ at the boundaries and "reflection boundary conditions" on the density, i.e., at the left edge $j = 1$, he sets $n_{j=0} = n_{j=2}$, and similarly for the right edge.

Thomas' problem has no net electric field i.e., $\phi_{left} = \phi_{right}$ or equivalently

$$\int_L E \cdot dx = 0 \ ;$$

hence, after predicting all E_j^n, he uses $(E_j^n - \overline{E_j^n})$ as his next guess: in this way he obtains convergence to E_j with zero average ($\overline{E_j} \to 0$).

The choice of which iterative scheme to use (the *expansion* scheme such as in Eq.(2), or the *direct* scheme of Eq.(5)) is of course dependent on the specific problem at hand. However some general statements can be made about their relative merits. One important consideration, for instance, might be the scheme's *convergence rate* to a solution. For the sample problems one of us has tried (V. T.), the first method of solution is significantly faster. This increased speed does become noticeable even for one dimensional simulations. This conclusion is consistent with the conclusions of Hockney and Eastwood [2], who showed that the first (expansion) method of solution has more desirable convergence properties than methods similar to the second (direct) method presented here. For higher dimensional problems the first method also has a natural extention and the improved convergence associated with that method might be decisive.

[2] R. W. Hockney and J. W. Eastwood, *Computer Simulation Using Particles*, Sec. 6.5 (McGraw-Hill International, 1981).

SECTION III: SUMMARY OF REPORTS, TALKS, VISITORS

Journal Articles:

Douglas Harned "Quasineutral Hybrid Simulation of Macroscopic Plasma Phenomena", *Jour. Comp. Phys*,47, pp.452-462, 1982.

Reports:

Y-J Chen, W.M. Nevins, C.K. Birdsall, "Stabilization of the Lower Hybrid Drift Instability by Resonant Electrons", UCRL-88305 (LLNL) Oct 28, 1982.

Talks:

At American Physical Society, Div. of Plasma Physics, Nov 1-5, 1982, New Orleans, LA. Abstracts follow this page.

Visitors:

Dr. Siegbert Kuhn, from Professor F. Cap's group at the Institute for Theoretical Physics, University of Innsbruck, arrived in December. He will be a guest researcher in our group for his sabbatical year(1983). He will be working on formalisms for handling finite, bounded systems and aiding us in our early efforts at simulating diode-like systems and sheath phenomena.

Temporal Development of a Plasma Sheath; Oscillatory vs. Steady State. Charles K. Birdsall, U. Calif. Berkeley CA 94720*—A uniform plasma of warm electrons and ions is placed in contact with a particle absorbing wall which is electrically floating. Many-particle 1d electrostatic simulation is used to follow the motion. There is no source so that the plasma eventually decays to the wall. The floating wall quickly becomes charged negatively; near the wall the particles are cooled, electrons reflected and ions accelerated, producing nearly equal electron and ion particle fluxes to the wall. During this transient state, the potential drop and the ion acceleration region (rarefaction wave) propagate at nearly v_{sound}, many λ_D into the plasma. The plasma-wall potential oscillates at ω_p about a mean value $\langle\phi\rangle$. The ion velocity at the wall falls between v_s and $\sqrt{2(q/m)_i\langle\phi\rangle}$. A wide range of parameters is used (m_i/m_e = 1 to 1600, $T_i/T_e = 10^{-4}$ to 64, L/λ_D=100,1000) Comparison is made to a fluid model with the same initial conditions but using warm electrons with an isothermal Boltzmann distribution and cold ions** in which the ions were found to enter the sheath at v_s.
*Work done at I.P.P., Nagoya, Japan and at Calif. Inst. Tech., Pasadena CA; supported in part by US DOE, ONR.
**J.W. Cipolla, M.B Silevitch, J. Plasma Phys. 25, 373, 1981.

ION-ION TWO-STREAM IN THERMAL BARRIERS: Vincent Thomas, U.C. Berkeley. We present studies of the electrostatic ion-ion two-stream instability as applied to thermal-barrier cells of a tandem mirror. The basis of our study is a model proposed recently by Cohen[1981] for the ion distribution function in such a cell. The results indicate that this instability should not present many difficulties for parameters of interest in the planned TMX-U and MFTFB tandem mirror experiments at LLNL. These results are quite different from an earlier study which used a less accurate ion distribution model taken from Lontano, Pekker and Pozzoli[1980].
Cohen, R. H., "Axial Potential Profiles in Thermal-Barrier Cells" Nuclear Fusion 21, 289[1981].
Lontano, M., Pekker, L. S. and Pozzoli, R. "Inverse-loss Cone Instability in a Tandem Mirror" Sov. J. Plasma Phys. 6, 432[1980].

Ion-Cyclotron Instability. NIELS F. OTANI, U.C. Berkeley. Computer simulations are made of the Alfvén ion-cyclotron (AIC) instability using two independent algorithms. One algorithm advances the vector potential on a 1-d grid parallel to B using the electron $E \times B$ term in Ampere's Law, while the other algorithm, based on D. Harned's quasineutral code, solves for the electric field on a 2-d grid using the electron momentum equation. Linear growth rates are found to agree with theory in the zero parallel temperature limit. Saturation and subsequent relaxation of the velocity distribution occur via a wave-breaking mechanism.
Harned, D. S. To appear in J. Comp. Phys.
Work supported by DOE.

DISTRIBUTION LIST

Department of Energy
Hitchkock, Katz, Lankford, Nelson, Sadowski

Department of Navy
Condell, Florance, Roberson

Austin Research Associates
Drummond, Moore

Bell Telephone Laboratories
Hasegawa

Cal. Inst. of Technology
Liewer

Calif. State Polytech. Univ.
Rathmann

Cambridge Research Labs
Rubin

Columbia University
Chu

E. P. R. I.
Scott

General Atomic Company
Bernard, Helton, Lee

Hascomb Air Force Base
Rubin

Hughes Aircraft Co., Torrance
Adler, Longo

Hughes Research Lab, Malibu
Harvey, Poeschel

JAYCOR
Hobbs, Klein, Tumolillo, Wagner

Kirtland Air Force Base
Pettus

Los Alamos National Lab.
Barnes, Borovsky, Forslund, Kwan, Lindemuth, Mason, Mostrom, Nielson, Oliphant, Sgro, Thode

Lawrence Berkeley Laboratory
Cooper, Kaufman, Kim, Kunkel, Lee, Pyle

Lawrence Livermore National Lab.
Albritton, Anderson, Brengle, Briggs, Bruijnes, Byers, Chambers, Chen, B.Cohen, Denavit, Estabrook, Fawley, Friedman, Freis, Fuss, Harte, Killeen, Kruer, Langdon, Lasinski, Maron, Matsuda, Max, Nevins, Nielsen, Smith, Tull

Mass. Inst. of Technology
Berman, Bers, Gerver, Hewett,

Mission Research Corporation
Godfrey

Naval Research Laboratory
Boris, Craig, Haber, Orens, Winsor

New York University
Grad, Harned, Weitzner

Northeastern University
Silevitch

Oak Ridge National Lab.
Dory, Meier, Mook

Princeton Plasma Physics Lab
Chen, Cheng, Lee, Okuda, Tang, Graydon

Sandia Labs, Albuquerque
Freeman, Humphries, Poukey, Quintenz, Wright

Sandia Labs, Livermore
Marx

Science Applications, Inc.
Drobot, Mankofsky, McBride, Siambis, Smith

Stanford University
Blake, Buneman

University of Arizona
Morse

University of California, Berkeley
Arons, Chen, Chorin, Grisham, Hudson, Keith, Lichtenberg, Lieberman, McKee, Morse, Birdsall, Crystal, Kim, Kuhn, Lawson, Otani, Thomas, Wendt

University of California, Davis
DeGroot, Woo

University of California, Irvine
Rynn

University of California, Los Angeles
Dawson, Decyk, Huff, Lin

University of Iowa
Knorr, Nicholson

University of Maryland
Guillory, Rowland, Winske

University of Pittsburgh
Zabusky

University of Texas
Horton, McMahon, Tajima

University of Washington
Potter

University of Wisconsin
Shohet

Varian Associates
Helmer

Bhabha Research Centre
Aiyer, Gioel

Culham Laboratory
Eastwood, Roberts

Ecole Polytechnique, Lausanne
Hollenstein, Rousset

Ecole Polytechnique, Palaiseau
Adam

Centro de Electrodinamica, Lisbon
Brinca

Kyoto University
Abe, Jimbo, Matsumoto

Nagoya University
Kamimura

Max Planck Inst. für Plasmaphysik
Biskamp, Kraft

Osaka University
Mima, Nishihara

Oxford University
Allen

Risø National Labs
Lynov, Pécseli

Tel Aviv University
Cuperman

Tohoku University
Saeki, N. Sato

Universität Bochum
Schamel

Universität Innsbruck
Cap

Universität Kaiserslautern
Wick

University of Reading
Hockney

University of Tromsø
Trulsen


ATE
MED